SUPPLEMENT TO THE *WELDING JOURNAL*, JANUARY 2015
Sponsored by the American Welding Society and the Welding Research Council

Primary Chromium Carbide Fraction Control with Variable Polarity SAW

Increasing the fraction of time spent welding in DCEN compared to DCEP can increase the amount of primary carbides

BY S. D. BORLE, I. LE GALL, AND P. F. MENDEZ

ABSTRACT

Using alternating current (AC) when welding chromium carbide hardfacing alloys has a pronounced effect on the resulting welds. To examine exactly the effect of AC balance (fraction of time in electrode positive) on Fe-Cr-C hardfacing, six different samples were made varying from 50 to 75% balance in 5% increments. The heat input was found to increase from 3.82 to 4.30 kJ/mm and dilution along the centerline increased from 3.7 to 31.1%. The ultimate consequence of increasing the balance was a decrease in the volume fraction of primary carbides from 21 to 3% and a decrease in average diameter of carbides from 30.3 to 21.8 mm with the increase in balance. The increase in the volume fraction of carbides also coincided with microstructures that had higher percentages of hypereutectic microstructures that should lead to more uniform wear throughout the height of the hardfacing. The increase in volume fraction of carbides as the balance decreases should also increase the wear resistance. The use of AC waveform with balances near 50% gave microstructures expected to perform the best.

KEYWORDS

• Hardfacing • Surfacing • Cladding • Submerged Arc • Chromium Carbide

Introduction

In Canada alone, wear is estimated to cost $2.5 billion a year (Ref. 1). To cut down on the cost of wear, hardfacing is employed. Fe-Cr-C hardfacing is a surface treatment aimed at improving the surface properties of metals, in which a welded cladding is deposited onto the surface of a substrate to improve the part's resistance to wear. There are a number of different types of material systems that are employed in surfacing (Refs. 1, 2). This research focuses on Fe-Cr-C hardfacing.

Fe-Cr-C hardfacing is a surfacing technique applied to plain carbon steel and is used in circumstances where it may be undergoing wear caused by abrasion, impact, erosion, and corrosion (Refs. 3–6). Fe-Cr-C hardfacing is used in a large number of industries including mining, mineral processing, cement production, and pulp and paper manufacturing (Refs. 7–9). In oil sands operations its use includes crusher teeth, sizing screens, and centrifugal pumps, wear-plate for truck bed liners, and slurry transport pipelines (Refs. 6, 10–12). Fe-Cr-C hardfacing tends to be relatively inexpensive in comparison to other surfacing types such as tungsten carbide-based and certain polymer liners, which lends them to being used on the larger scale components (Ref. 12). This research examines Fe-Cr-C hardfacing produced with the submerged arc welding (SAW) process. The main reasons for using SAW over other processes are its high productivity and deposition rates (Ref. 13).

For the optimization of the production of Fe-Cr-C hardfacing, the use of square-wave alternating current (AC) is attractive because of its ability to control dilution and decrease heat input. The variables of AC waves that can be controlled are the balance, DC offset, and frequency. This research looks solely at the effect of controlling the balance, which has been identified as the most important waveform variable controlling dilution (Ref. 14). The balance is given as a percent of time the arc spends in electrode positive polarity. When using a constant-voltage (CV) implementation of AC welding, the wire feed speed (WFS) and the voltage are set and held constant while the machine varies the current (Ref. 14).

S. D. BORLE was a MSc. student at the University of Alberta at the time of this research and is currently at Group Six Technologies. I. LE GALL was a visiting student at the University of Alberta from Université de Nantes. P. F. MENDEZ is a professor and director at the Canadian Center for Welding and Joining at the University of Alberta, Canada.

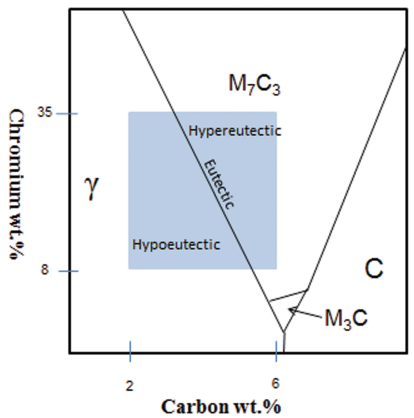

Fig. 1 — Idealized liquidus surface of the Fe-Cr-C ternary phase diagram.

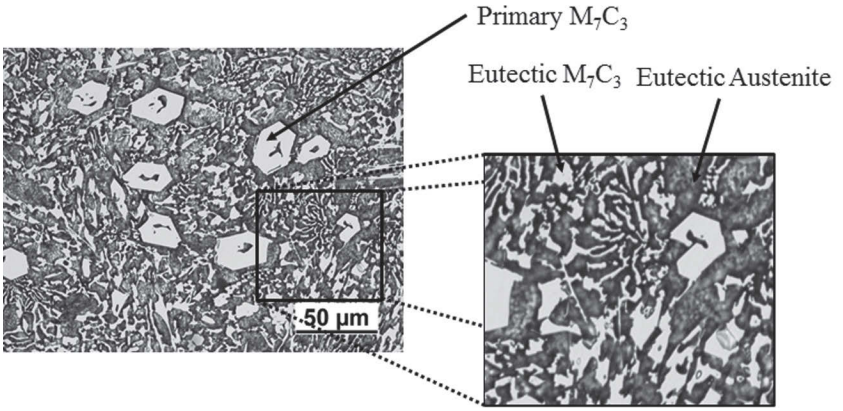

Fig. 2 — Hypereutectic microstructure showing large hexagonal M_7C_3 primary carbides surrounded by a matrix of eutectic M_7C_3 and austenite.

Table 1 — Balance Settings Used in This Work

Sample	Balance
A	50
B	55
C	60
D	65
E	70
F	75

Microstructure of SAW Chromium Carbide Surfacing

The compositions of the Fe-Cr-C hardfacing tend to fall in the ranges of 8–35 wt-% Cr and 2–6 wt-% C (Refs. 3, 13, 15, 16). As shown in the idealized pseudo ternary in Fig. 1, this range of compositions encompasses three distinct categories of microstructure: hypoeutectic, eutectic, and hyper-eutectic. There is a large difference between the microstructures and the mechanical properties of the three different categories. Hypereutectic alloys' wear resistance is normally superior (Ref. 2), but corrosion resistance and toughness are often better in hypoeutectic alloys (Refs. 13, 17).

Microstructure of hypereutectic alloys consists of primary M_7C_3 carbides surrounded by a matrix of eutectic austenite and eutectic M_7C_3 carbides. The hexagonal M_7C_3 carbides solidify first, as the composition of the melt approaches the eutectic line and the temperature decreases, the solidification changes to eutectic M_7C_3 carbides and austenite (Ref. 17). An example of the typical microstructure is shown in Fig. 2. The size of the primary carbides increases as the cooling rate decreases or chromium wt-% increases, while the addition of carbon increases the volume fraction of carbides while refining them (Refs. 15, 18).

When the composition of the alloy falls at or close to the eutectic line, M_7C_3 and austenite (γ) solidify simultaneously as a eutectic microstructure (Ref. 19). Figure 3 is an example of a eutectic microstructure in chrome carbide surfacing. The eutectic can either be a rosseta-like morphology, as shown in Fig. 3, or it can be fibrous bundles (Refs. 20, 21).

When the composition is in the austenite region of the ternary, the resulting microstructure is hypoeutectic. In this case, the solidification starts as primary austenite dendrites and then as a eutectic of M_7C_3 and austenite (Refs. 19, 22). The austenite dendrites are surrounded by the eutectic microstructure of M_7C_3 carbides and austenite, as seen in Fig. 4.

Previous work has shown there can be a large variance in the wear resistance within the different microstructures and compositions of Fe-Cr-C hardfacing; however, it is generally agreed that as composition varies from hypereutectic to eutectic to hypoeutectic, the wear resistance decreases (Refs. 2, 10–12, 17, 23–28). A significant part of the wear resistance increase going from hypoeutectic to eutectic to hypereutectic microstructures is attributed to the increase in the amount of carbides. In hypereutectic alloys, an increase in the surface fraction of primary carbides increases wear resistance (Ref. 7).

An entirely hypereutectic microstructure is wanted for the best possible abrasion resistance, but traditional hypereutectic alloys can contain all three microstructures (Refs. 2, 29, 30). Figure 5 is an example of how the microstructure of a SAW Fe-Cr-C hardfacing can be hypereutectic at the top, eutectic in the middle, and hypoeutectic close to the weld interface. This variation is representative of Fe-Cr-C hardfacings in general, and it is not typically seen in cast structures of similar compositions. Figure 5 was taken from micrographs of an unetched sample taken using BSE imaging.

This layering occurs because of differences in composition along the height of the weld (Ref. 29). However, it is unclear between solidification, segregation, diffusion, lack of mixing, and diffusion what the main cause is. The issue with the layering is the wear resistance will not be uniform throughout the service life of the hardfacing. Testing protocols address these variations by specifying a particular depth at which wear testing must be performed (e.g., 75% of cladding depth). Current research is being performed in order to generate a better understanding of layering, which has very important practical consequences. This paper focuses on how a balance in a square waveform affects the amount of primary carbides and the physical cause for this phenomenon.

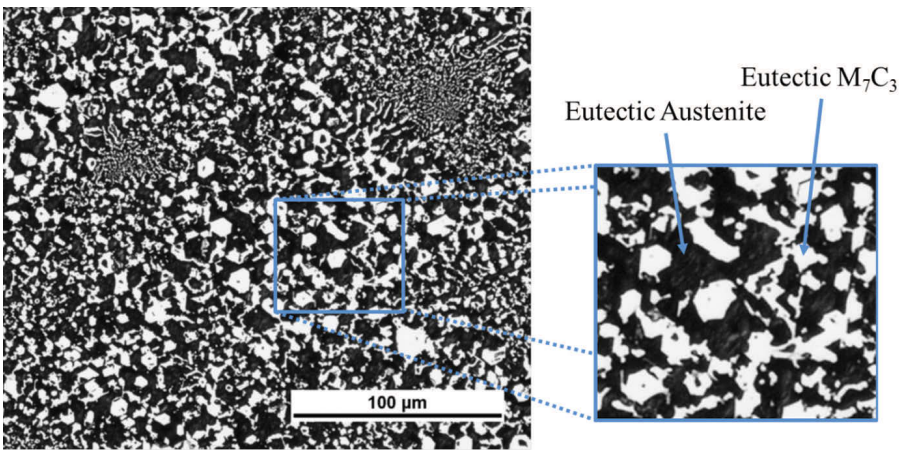

Fig. 3 — Eutectic microstructure of austenite and M_7C_3.

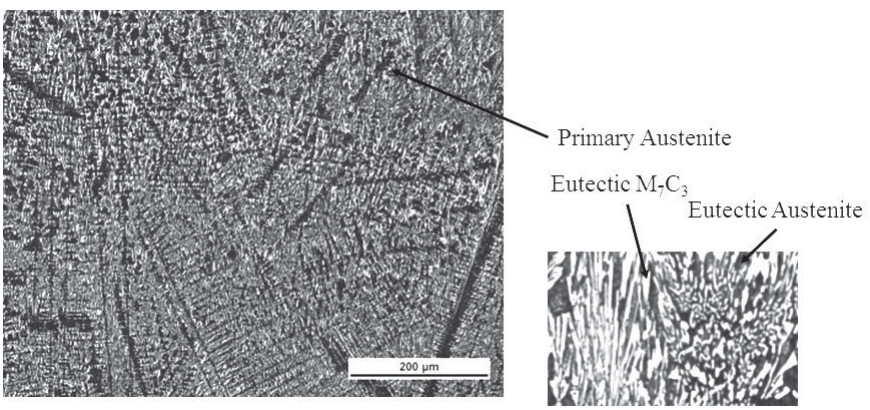

Fig. 4 — Hypoeutectic microstructure of primary austenite dendrites surrounded by eutectic M_7C_3 and austenite.

Table 2 — Summary of Dilution and Heat Input for AC Balances between 50 and 75%

Sample	Balance (%)	Dilution Center (%)	Dilution Side (%)	Heat Input kJ/in. (kJ/mm)
A	50	3.7	34.0	97 (3.82)
B	55	4.8	32.8	100 (3.96)
C	60	19.7	47.5	101 (4.00)
D	65	18.7	38.6	103(4.06)
E	70	25.7	41.3	108 (4.23)
F	75	31.1	41.4	109 (4.30)

Experimental Procedure

When producing Fe-Cr-C hardfacing using SAW, an alloying powder that contains elements such as chromium, carbon, manganese, and molybdenum is placed down in front of the welding head. The powder used for the current research was based on a proprietary blend used to produce Fe-Cr-C hardfacing industrially. The main alloying elements were chromium and carbon with lesser amounts of manganese, silicon, molybdenum, and boron added. A welding gun attached to a weaving mechanism was used to produce passes of the desired width. Setups used to produce Fe-Cr-C hardfacings resemble the schematic shown in Fig. 6. In the case of the current research, only a single weld bead was deposited and the powder was applied evenly by using a wheel feeder rotating at a constant speed while traveling along the path of the weld previous to actually welding. In these experiments, single weld beads of 1¾ in. (44.5 mm) width were made on a 9 × 12-in. (228 × 305-mm) A36 plate with a thickness of $\frac{5}{16}$ in. (7.94 mm). The sample plate was clamped to the base plate using bolts going through ½-in.-thick plates on top of the sample plates with the bolts threaded into the base plate to prevent distortion of the sample plate when welding.

Typical operating ranges for welding of Fe-Cr-C hardfacing using SAW are 30–40 V and 500–700 A. The other operating parameters such as wire feed speed, alloy powder addition, and weave are chosen to ensure proper melting of the powder, a good surface finish, and slag detachability. The basis of the welding parameters were chosen to replicate an industrially produced product with the balance being the only welding variable changing between the samples. The flux used for these experiments was 1.5 on the basicity index. The experimental settings were chosen to resemble an industrially produced product and to examine the possibility of process/product improvement. The welding was done with constant voltage, constant wire feed speed, and constant translation velocity, so that the ratio of wire to powder was constant through all the welds. The offset was not adjusted, the frequency was kept constant at 45 Hz, and no preheat was applied to the base metal. The samples and their respective balance settings are listed in Table 1.

The consumables used were an agglomerated basic flux along with a L-61 welding wire (EM12K). A proprietary blend of powders was used to produce a weld metal high in chromium and carbon. The power source used was an AC/DC SAW machine that allowed for the manipulation of AC waveforms along with data acquisition through a built-in program. The waveform data collected by the machine were then used to determine the HI of the welds. HI was calculated by taking the average of the instantaneous power throughout welding. Dilutions of the samples were measured using the formula shown in Equation 1 and with the areas described in Fig. 7 (Ref. 24).

$$Dilution(\%) = DA/(DA + OA) \times 100 \quad (1)$$

DA is the area of dilution or the amount of the base metal that was melted, and OA is the area of the over-

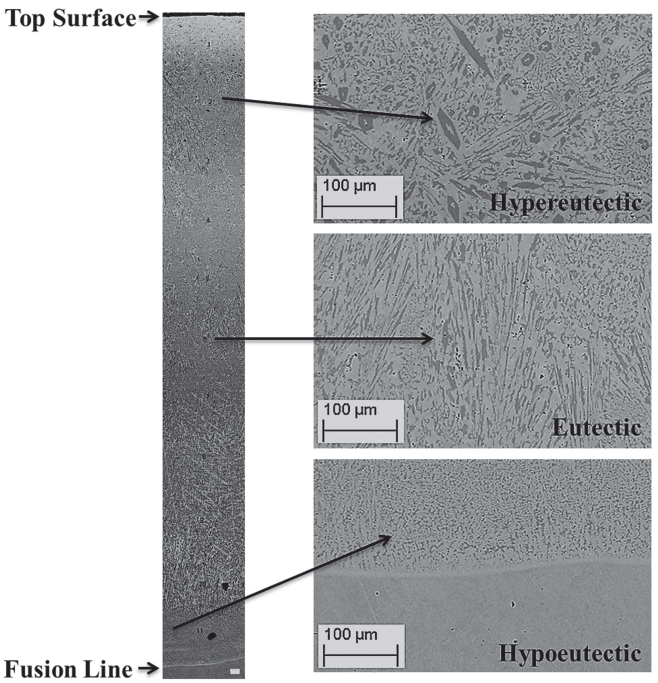

Fig. 5 — Microstructure of chromium carbide surfacing showing a microstructural variation of hypereutectic at the top, eutectic in the middle, and hypoeutectic at the bottom.

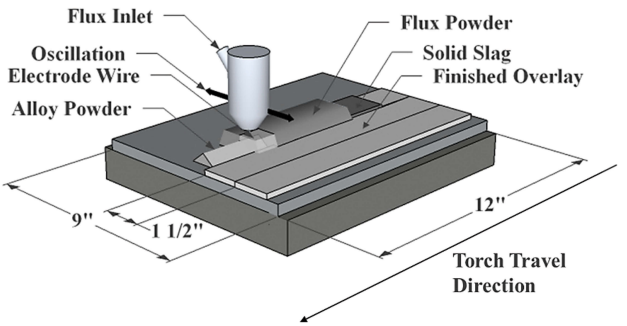

Fig. 6 — Schematic of the experimental SAW setup for the Fe-Cr-C hardfacing used in this work.

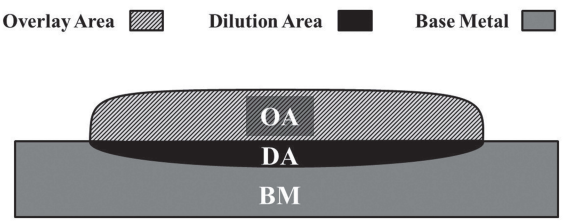

Fig. 7 — Schematic of transverse cross section of a chromium carbide surfacing highlighting the cladding area, the dilution area, and the base metal.

lay that has been added.

To calculate the dilution measurements, samples were taken along the sagittal plane of the weld at the centerline and 15 mm off to the side, as shown in Fig. 8, to account for the lack of uniformity of the welds. The zig-zag line in Fig. 8 represents the weaving pattern in the deposition of a single bead.

Metallographic samples for volume fraction measurements were made from along the longitudinal center of the welds, while dilution measurements were taken from samples taken from the transverse of the welds. The samples were hot mounted in Bakelite® and then ground and polished using an automatic polisher with 22.24 N force. For the first step, 60-grit rough grinding was carried out for 5 min. After this, multiple other grinding passes down to 1200 grit were carried out at 3 min for each stage. The samples were then polished using a 1-µm diamond suspension for 5 min. All of the micrographs with exception of those shown in Fig. 5 were etched for 30 s using a mixture of 20 mL deionized water, 10 mL HCl, 30 mL HNO_3, and 5 g $FeCl_3$.

In order to get a good representation of the microstructure, a large number of photographs was taken of samples that were then photo merged together to make large micrographs across a large width and the entire height of the weld. The total volume fraction of carbides was then measured by using Photoshop® to select all of the light areas of the microstructure in the weld pool with the exception of the unfused powders, which were not included in the volume fraction analysis or size analysis. For the samples where the primary carbides' volume fraction and size were measured, smaller areas from the large micrograph were examined. The primary carbides in the smaller areas were then selected and the total area of the carbides measured using Photoshop. The average size of the primary carbides in the individual micrographs was then calculated by dividing the area by the number of carbides selected. The average size of primary carbides in the sample was calculated by taking the total number of all the carbides that had been measured throughout the smaller micrographs divided by the total area of all of those carbides that were measured. The diameter given is the distance between two parallel sides if the carbides are represented as regular hexagonal shaped.

Results

Figure 9 shows how the profiles vary when cut transversely across the samples. The concave weld interface observed is a result of the weaving, which has a longer dwell time at the edges than at the center of the weld. These cross sections show that the penetration is increasing throughout the samples as the balance increases. The actual dilution measurements were taken from the longitudinal sections and are tabulated in Table 2 along with the heat input calculations.

Figure 10 shows that the trend for the heat input and dilution is to increase as the balance increases. The exception is at 60% balance, which showed exceptionally high dilution amounts in the experiments performed. The sides are less sensitive to variations of balance. One possible reason for this observation is that the larger depth of molten metal at the sides reduces the efficiency of cathodic heating on the weld bead.

The influence of balance in the microstructural inhomogeneity across

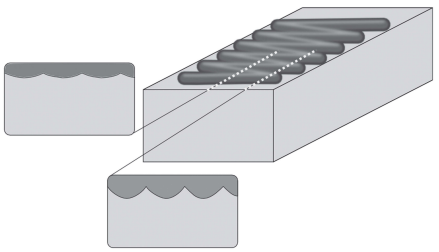

Fig. 8 — Schematic of dilution measurement locations taken along the longitudinal of the weld hardfacing.

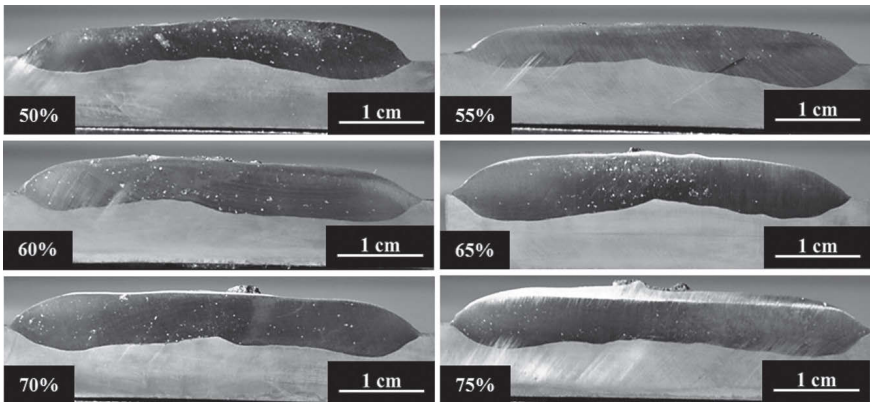

Fig. 9 — Cross sections of single bead Fe-Cr-C hardfacing for AC balance between 50 and 75%.

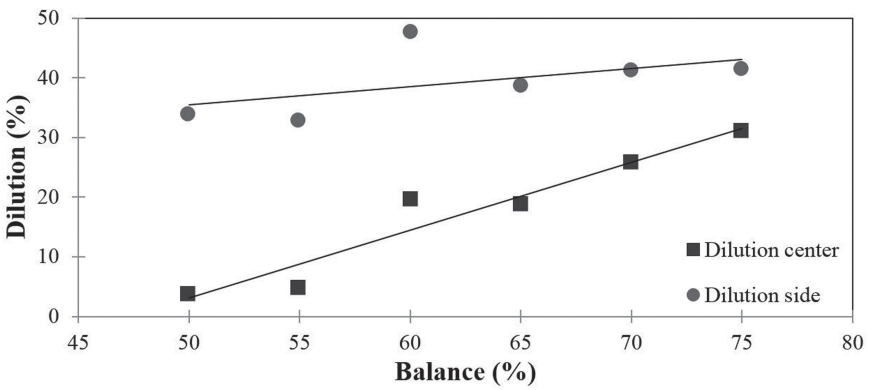

Fig. 10 — Variation of dilution with AC balance.

the depth of the hardfacing is illustrated in Fig. 11. For all images, the top corresponds to the free surface of the bead, and the bottom corresponds to the weld interface. For all balances, a hypereutectic structure is observed at the top, and often a hypoeutectic structure near the weld interface. The white round features correspond to powders that were not completely molten, some of which reach a large size, of the order of 1 mm (seen in the 60% balance image). A steady decrease in the amount of hypereutectic microstructure at the top was observed with the increase in balance.

Figure 12 presents a higher magnification image of areas of hypereutectic composition from the cross sections in Fig. 11. Because of the small size covered by each image, conclusions about primary carbide fraction were made by direct measurement over a number of different areas.

The measured volume fraction (VF) of hypereutectic microstructure, total carbide VF, VF of primary M_7C_3 carbide, and the average primary M_7C_3 size are given in Table 3 and Fig. 13.

Figure 13 illustrates graphically the trends determined, showing how the amount of microstructure that is hypereutectic goes from under half to 100% as the balance reaches 50%. The volume fraction and average primary carbide size increases as the balance decreases. The decrease in primary carbide fraction is consistent with the increase in dilution.

Discussion

The steady decrease in primary carbide fraction with balance is consistent with the well-known effect of increased dilution with balance, coupled with the understanding of the thermodynamics of the material system used. The increase in dilution with balance is due to the metal spending increasing amounts of time as a nonthermionic cathode, with the associate heat input on the surface (Refs. 32, 33). The reduction in the amount of primary carbides with a reduction of Cr and C in the system has been reported previously (Refs. 15, 18, 22). Although no wear tests were performed for the samples prepared, it is to be expected that the increase in primary carbides should increase the wear properties of the chromium carbide surfacing (Refs. 11, 15). Another effect of decreasing the balance was to increase the volume fraction of the hypereutectic microstructure, which should make the wear resistance more uniform throughout the height of the cladding.

It is not clear at this time why for the intermediate value of 60% balance the dilution departed from the general trend observed. Metallographic measurements of carbide fraction and size did not show an equivalent departure in the trends.

The decrease in size of primary carbides with the reduction of balance was unexpected, and opposite of what would be expected from welds with higher heat input. Other experiments performed with similar alloy systems showed very little variation in carbide size for a wide range of heat inputs. The effect observed here could be because of an increase in the amounts of Mo and Si caused by the decrease in the dilution, as both have been found to reduce the rate of carbide precipitation, which could lead to the larger carbides (Refs. 29, 31).

This work did not test the effect of offset and frequency on the microstructure. Based on previous studies (Ref. 14), it is reasonable to expect that offset will be of secondary importance (with a slight decrease in fraction of primary carbides with an offset biased toward

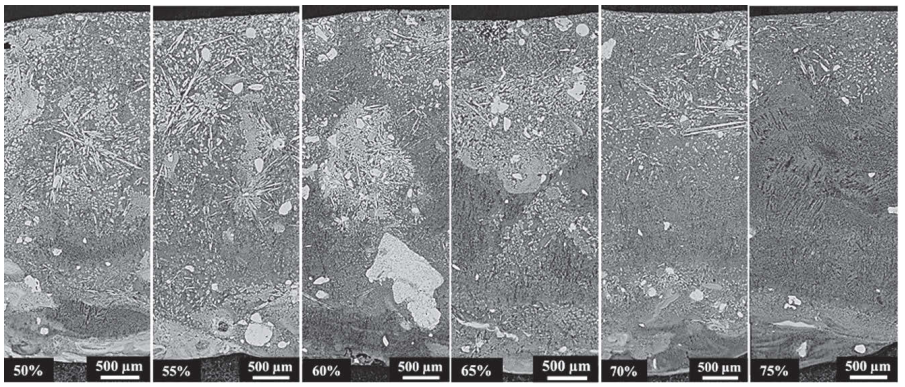

Fig. 11 — Longitudinal sections of hardfacing with AC balances between 50 and 75%.

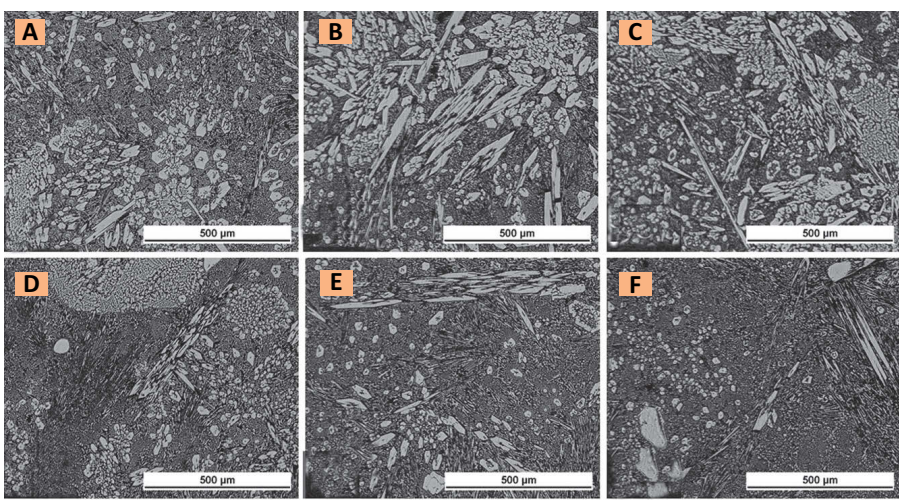

Fig. 12 — High magnification of hardfacing with AC balances between 50 and 75%. A — 50%; B — 55%; C — 60%; D — 65%; E — 70%; F — 75%.

Table 3 — Microstructural Characterization Measurements of Carbides

Balance (%)	Total VF Carbide (%)	VF Hypereutectic (%)	VF Pimary M_7C_3 (%)	Average Diameter (µm)
50	45.8	100.0	21	30.3
55	42.7	100.0	20	26.7
60	32.8	100.0	18	24.9
65	37.8	84.8	14	23.0
70	31.4	75.6	9	22.7
75	21.0	40.3	3	21.8

DCEP). No effect is expected with frequency changes until frequencies are so high that the ramp-up and ramp-down time is of duration comparable to the hold time. In this case, heat input would be reduced, likely resulting in lower dilution and higher carbide fraction. Such high frequencies are not recommended though because of the difficulty in controlling the process accurately in that range.

Somewhat similar effects to the ones reported here are also expected by varying the contact tip-to-workpiece distance (CTWD) while keeping the same voltage and wire feed speed. Longer CTWD should have a comparable effect to decreased balance, resulting in a higher carbide fraction. Adjusting CTWD involves mechanical adjustments that are often undesirable in the large equipment typically used in producing a Fe-Cr-C hardfacing.

Balances below 50% were also considered informally in this work, but the slag system used was too difficult to remove, and it was considered impractical for industrial use.

Conclusion

This work assessed for the first time the effect of balance on AC waveform in the SAW of Fe-Cr-C hardfacing. The practical implications of the findings are very significant because Fe-Cr-C hardfacing is the most commonly used approach to wear protection in ground engagement equipment in mining, oil, gas, and logging industries.

The amount of primary carbides increases steadily with a decrease in balance. The cases studied indicated a primary carbide fraction increase from 3% for a 75% balance to 21% for a 50% balance. This effect is directly related to the decrease in dilution as the balance decreases.

The size of primary carbides also increased with the reduction of balance, from a characteristic size of 21.8 µm for 75% balance to 30.3 µm for a 50% balance. This work also showed how the layered structure of Fe-Cr-C hardfacing is present in a wide range of balances and how it can be affected by altering the balance. Balances of 60% and below resulted in pure hypereutectic microstructures. A hypereutectic structure throughout the hardfacing thickness is expected to help make it reliable with good wear resistance even at advanced stages of wear.

Acknowledgments

The authors want to acknowledge the support of Wilkinson Steel and Metal, Lincoln Electric, and NSERC.

References

1. Mendez, P. F., Barnes, N., Bell, K., Borle, S. D., Gajapathi, S. S., Guest, S. D., Izadi, H., Gol, A. K., and Wood, G. 2014. Welding processes for wear resistant overlays. *Journal of Manufacturing Processes*. pp. 4–25.

2. Kotecki, D. J., and Ogborn, J. S. 1995. Abrasion resistance of iron-based hardfacing alloys. *Welding Journal* 74(8): 269-s to 278-s.

3. Azimia, G., and Shamanian, M. 2010. Effects of silicon content on the microstructure and corrosion behavior of Fe-Cr-C hardfacing alloys. *Journal of Alloys and Compounds* (502): 598–603.

4. Chang, C.-Ming, Hsieh, C.-Chun, Lin,

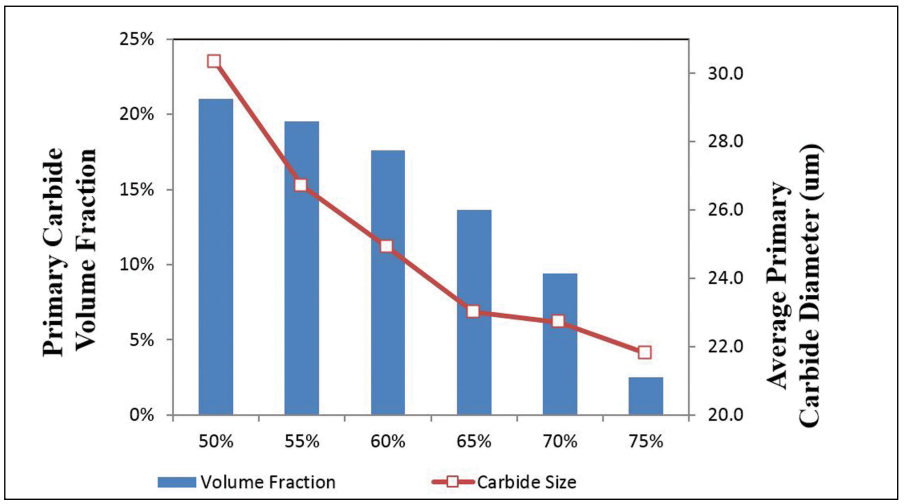

Fig. 13 — Primary carbide volume fraction and average primary carbide size.

C.-Ming, Chen, J.-Hao, Fan, C.-Ming, and Wu, W. 2010. Effect of carbon content on microstructure and corrosion behavior of hypereutectic Fe-Cr-C claddings. *Materials Chemistry and Physics*.

5. Chotěborský, R., Hrabě, P., Müller, M., Válek, R., Savková, J., and Jirka, M. 2009. Effect of carbide size in hardfacing on abrasive wear. *Research in Agricultural Engineering* 55(4): 149–158.

6. Kirchgaßner, M., Badisch, E., and Franek, F. 2008. Behaviour of iron-based hardfacing alloys under abrasion and impact. *Wear* (265): 772–779.

7. Chang, C.-Ming, Chen, L.-Hsien, Lin, C.-Ming, Chen, J.-Hao, Fan, C.-Ming, and Wu, W. 2010. Microstructure and wear characteristics of hypereutectic Fe-Cr-C cladding with various carbon contents. *Surface & Coatings Technology* (205).

8. Dogan, O. N., Hawk, J. A., and Laird, G. 1997. Solidification structure and abrasion resistance of high chromium white irons. *Metallurgical and Materials Transactions A — Physical Metallurgy and Materials Science* 28(6): 1315-1328. doi —10.1007/s11661-997-0267-3.

9. Lin, C.-Ming, Lai, H.-Han, Kuo, J.-Chao., and Wu, W. 2011. Effect of carbon content on solidification behaviors and morphological characteristics of the constituent phases in Cr-Fe-C alloys. *Materials Characterization* 62(12): 1124–1133. doi —10.1016/j.matchar.2011.09.007.

10. Flores, J. F., and Neville, A. Materials selection in the oilsands industry based on materials degradation mechanisms. *Exploration and Production* 7(1): 42–45.

11. Flores, J. F., Neville, A., Kapur, N., and Gnanavelu, A. 2009. Erosion-corrosion degradation mechanisms of Fe-Cr-C and WC-Fe-Cr-C PTA overlays in concentrated slurries. *Wear* (267): 1811–1820.

12. Fisher, G., Wolfe, T., Yarmuch, M., Gerlich, A., and Mendez, P. 2012. The use of protective weld overlays in oil sands mining. *Australasian Welding Journal* 57(2): 12.

13. Mellor, B. G. 2006. *Welding Surface Treatment Methods for Protection against Wear*. Ed., B. G. Mellor.

14. Pepin, J. 2009. Effects of submerged arc weld (SAW) parameters on bead geometry and notch-toughness for X70 and X80 linepipe steels. Thesis, University of Alberta, Canada.

15. Chang, C.-Ming, Chen, Y.-Chun, and Wu, W. 2010. Microstructural and abrasive characteristics of high carbon Fe-Cr-C hardfacing alloy. *Tribology International* pp. 929–934.

16. Hinckley, B., Dolman, K. F., Wuhrer, R., Yeung, W., and Ray. A. 2008. SEM investigation of heat treated high-chromium cast irons. *Materials Forum* 32: 55–71.

17. Neville, A., Reza, F., Chiovelli, S., and Revega, T. 2006. Characterization and corrosion behavior of high-chromium white cast irons. *Metallurgical and Materials Transactions A — Physical Metallurgy and Materials Science* 37A(8): 2339–2347. doi —10.1007/BF02586208.

18. Zhou, J., and Jincheng, L. 2011. Colour metallography of cast iron. *SCI* 8 (1).

19. Schon, C. G., and Sinatora, A. 1998. Simulation of solidification paths in high chromium white cast irons for wear applications RID F-1494-2010 RID B-5107-2010. *Calphad-Computer Coupling of Phase Diagrams and Thermochemistry* 22(4): 437–448. doi —10.1016/S0364-5916(99)00003-6.

20. Dogan, O. N. 2005. Effect of chemical composition and superheat on the macrostructure of high Cr white iron castings. Albany Research Center. U.S. Department of Energy.

21. Powell, G. L. F., Brown, I. H., and Nelson, G. D. 2008. Tough hypereutectic high chromium white iron — A double in-situ fibrous composite. Eds. J. Yan Bell, C. Ye, and L. Zhang. *Advanced Materials Research* 32: 111–114.

22. Tabrett, C. P., Sare, I. R., and Ghomashchi, M. R. 1996. Microstructure-property relationships in high chromium white iron alloys. *International Materials Reviews* 41(2): 59–82.

23. Liu, Z. J., Su, Y. H., and Sun, J. G. 2008. Effects of shape and distribution of M_7C_3 on wear resistance of iron based composite. Eds. M. K. Zhu, X. P. Lei, and K. W. Xu. *Key Engineering Materials* 373-374: 560–563.

24. Klimpel, A., Dobrzanski, L. A., Janicki, D., and Lisiecki, A. 2005. Abrasion resistance of GMA metal cored wires surfaced deposits. *Journal of Materials Processing Technology* 164 (5): 1056–1061. doi —10.1016/j.jmatprotec.2005.02.242.

25. Zhou, Y. F., Yang, Y. L., Jiang, Y. W., Yang, J., Ren, X. J., and Yang, Q. X. 2012. Fe-24 wt.%Cr-4.1 wt.%C hardfacing alloy — Microstructure and carbide refinement mechanisms with ceria additive. *Materials Characterization* 72(10): 77–86. doi —10.1016/j.matchar.2012.07.004.

26. Buytoz, S. 2006. Microstructural properties of M_7C_3 eutectic carbides in a Fe-Cr-C alloy. *Materials Letters* 60(5): 605–608.

27. Wang, Q., and Li, X. 2010. Effects of Nb, V, and W on microstructure and abrasion resistance of Fe-Cr-C hardfacing alloys. *Welding Journal* 89(7): 133-s to 139-s.

28. Buchely, M. F., Gutierrez, J. C., Leon, L. M., and Toro, A. 2005. The effect of microstructure on abrasive wear of hardfacing alloys. *Wear* 259(1): 52–61.

29. Powell, G. L. F., Carlson, R. A., and Randle, V. 1994. The morphology and microtexture of M_7C_3 carbides in Fe-Cr-C and Fe-Cr-C-Si alloys of near eutectic composition. *Journal of Materials Science* 29(9): 4889–4896. doi —10.1007/BF00356539.

30. Atamert, S., and Bhadeshia, H. K. D. H. 1990. Microstructure and stability of Fe-Cr-C hardfacing alloys. *Materials Science and Engineering* — A 130 (1): 101–111. doi —10.1016/0921-5093(90)90085-H.

31. Pearce, J. T. H. 1984. Structure and wear performance of abrasion resistant chromium white cast irons. *American Foundry Society Transaction* 84: 599–622.

32. Lancaster, J. F.. 1984. The physics of welding. *Physics in Technology* 15(2): 73.

33. Lincoln Electric. 2008. *Submerged Arc Welding Guide*. The Lincoln Electric Co., Cleveland, Ohio.